IEEE Access
Multidisciplinary | Rapid Review | Open Access Journal

Received 14 April 2023, accepted 2 May 2023, date of publication 4 May 2023, date of current version 16 May 2023.

Digital Object Identifier 10.1109/ACCESS.2023.3273120

APPLIED RESEARCH

A Miniaturized Harmonic Reject Waveguide Filter for Ku-Band VSAT Transmitter

XUEJIAN JIANG, ZHENGBIN XU, JIE XU, JIAN GUO, (Member, IEEE), AND CHENG QIAN
State Key Laboratory of Millimeter Waves, School of Information Science and Engineering, Southeast University, Nanjing 210096, China
Corresponding author: Zhengbin Xu (zb_xu@seu.edu.cn)

ABSTRACT In this paper, a novel miniaturized low-pass waveguide filter with wide stop-band is proposed for the harmonic rejection of Ku-band Very Small Aperture Terminal (VSAT) transmitters. The proposed filter consists of a corrugated waveguide low-pass filter and a metal septum in the H-plane at the center of the narrow side wall. Because it does not require additional impedance transformers, the proposed filter achieves a compact size. To estimate the amplitude level of the higher-order modes at the input port of the harmonic reject filter in a RF transmitter, higher-order modes generated by E-plane probe-type microstrip-to-waveguide (M2W) transition are analyzed and calculated using commercial numerical tools. To analyze the response of the proposed filter in higher-order modes, the mode conversions in the structure are also analyzed and calculated. The analysis shows that a wide stop-band free of spurious response in all higher-order modes can be obtained by co-designing M2W transition and filter. To validate the design concept, a Ku-band harmonic reject filter is designed using WR-75 waveguide. Simulation results show that the reflection is less than −23dB between 13∼15 GHz, while the suppression stop-band performance in TE_{10} mode is better than 35dB in 17.5∼29.6 GHz. The effective length of the filter is 29 mm. Simulation results also indicate that the spurious pass-band performance in TE_{20}, TE_{21} and TM_{21} modes is improved by the M2W transition. Finally, to validate the proposed idea, a Ku-band GaN power amplifier is fabricated and measured. The measurements show that the amplifier has a minimum output power of 72.5 W with better than 20 dBc 2nd harmonic rejection. By using the proposed filter, the measured 2nd harmonic rejection of the power amplifier is greater than 52 dBc.

INDEX TERMS Harmonic reject, miniature, waveguide filter, higher-order mode, VSAT transmitter.

I. INTRODUCTION

In recent decades, very small aperture terminal (VSAT) networks have spread throughout the world [1], [2], [3], [4]. The demand for small VSAT transceivers has increased because of their portability, low cost and high reliability. To meet the requirements of high-speed data communications, high power transmitters are necessary. In Ku-band, a single internally matched GaN power amplifier can deliver up to 70 W of output power [5]. Moreover, by employing power combining technology, output power of a Ku-band transmitter can reach hundreds of watts. It is well known that GaN power amplifiers typically operate in saturation or even deep saturation state. As a result, high-level harmonic components, especially the second harmonic, are generated due to nonlinear effects. The typical transmitting frequency band of Ku-band VSAT station is 13.75∼14.5 GHz [6]. Therefore, the second harmonic lies in the range of 27.5∼29 GHz, which is the frequency band allocated for Ka-band satellite communication and 5G communication applications [6], [7], [8]. To avoid interference with other equipment, the power level of the second harmonic should be as low as possible.

Compared with planar filters, waveguide filters have the advantages of high-quality (Q) factor, low insertion loss, high power capability, etc. These features are particularly attractive for low-loss and high-power applications. However, it is difficult to design a rectangular waveguide filter with a wide stop-band. The narrow stop-band bandwidth is insufficient to cover the harmonic frequencies [9], [10], [11]. In addition, higher-order modes are always generated in a high-power

The associate editor coordinating the review of this manuscript and approving it for publication was Mohamed M. A. Moustafa.

RF transmitter due to the discontinuities, such as microstrip-to-waveguide (M2W) transitions, waveguide bends, impedance transformers, and so on. Therefore, the rejection performance of higher-order modes is also a key issue in the design of harmonic suppression filters.

To suppress the harmonic frequencies generated by RF transmitters, a waffle-iron filter is proposed [12]. A stop-band bandwidth of 6 octaves is achieved by cascading three different waffle-iron filters with staggered stop-bands. However, the relatively low power handling capability limits the application of this filter. The corrugated waveguide filter [13], [14] is also a classical solution because of its high-power handling capability and wide stop-band in TE_{10} mode. However, when the filter is excited by the higher-order modes (TE_{n0}, n > 1), narrow spurious components or "spikes" caused by the higher-order modes are observed in the stop-band. The spikes cannot be eliminated, whereas they can be moved out of the critical frequency ranges by applying iterative optimization procedure [15]. To improve the rejection performance, an inhomogeneous corrugated waveguide is proposed [16]. In this case, the higher-order spurious spikes are significantly improved, nevertheless, they still locate in the stopband. The suppression of higher-order modes is further improved by using a composite corrugated filter [17], consisting of two cascaded corrugated filters with different waveguide widths. However, the overall length of this design is also increased. It should be mentioned that, both of the waffle-iron and corrugated filters have very low input/output port impedances to avoid the propagation of TE_{0m} modes. It means that additional impedance transformers are required to match these filters to full-size waveguides, resulting in a larger size.

To alleviate the above issues, evanescent-mode ridged waveguide filters are proposed [18], [19]. Similar to the waffle-iron filter, the ridged filter requires very small gap sizes to achieve adequate out-of-band rejection. Therefore, its power-handling capability is limited. Moreover, additional impedance transformers are also necessary to match the ridged waveguide housing.

On the other hands, filters consisting of a quasi-periodic E-plane band-stop elements of sinusoidal profile have been studied in the past decades [20], [21], [22]. The filter can achieve a wide spurious-free TE_{10} mode frequency response and higher-order TE_{n0}-mode suppression. In [22], a Ku-band high power low-pass filter show a 60-dB rejection level from 13.75 GHz and up to 40 GHz in TE_{10} mode, while all higher-order modes are suppressed. However, the overall length of this filter is 218 mm, which is unsuitable for applications of miniaturized transmitter. Furthermore, it is difficult to manufacture such filters using low-cost computer-controlled milling. To solve this problem, stepped band-stop elements are used instead of sinusoidal profile elements in [23] and [24].

It is well known that, in filter design, there is generally a trade-off between stop-band performance and physical size. Therefore, if the filter is designed according to the output characteristics of the amplifier, such as higher-order mode levels, compact size and harmonic suppression performance can be achieved simultaneously.

In this paper, a miniaturized waveguide harmonic reject filter is proposed. The principle is illustrated and the mode conversion is analyzed in Section II. Following that, the higher-order mode transmission characteristic of the E-plane M2W transition is analyzed in Section III. To validate the proposed design concept, a Ku-band harmonic reject filter is designed using WR-75 waveguide. As a practical demonstration, a Ku-band transmitter prototype consisting of a power amplifier module and the proposed filter is designed, fabricated and experimentally validated in section IV. The measurement results show that the 2nd harmonic rejection performance of the transmitter is significantly improved by the proposed filter.

II. MINIATURIZED WAVEGUIDE LOW-PASS FILTER

A. STRUCTURE AND PRINCIPLE

As shown in Fig.1, the proposed waveguide low-pass filter consists of normal input/output waveguide port, together with a corrugated waveguide low-pass filter with a H-plane septum at the center of the narrow side wall. To simplify the analysis, an equivalent circuit model is proposed as shown in Fig.1(d). The proposed waveguide filter can be divided into three parts along the signal propagation direction: the power divider, the main filter and the power combiner. Firstly, the power divider splits the input signal into two components with equal amplitude. Different with conventional power dividers, the output impedance is only half of the input port, and therefore, impedance transformers are no longer required for port matching. Secondly, the main filter part consists of two identical low-pass filters, which mainly determines the overall performance of the proposed filter. Thirdly, the structure of the power combiner is the same as that of the power divider, but the functions are reversed.

Fig.2 shows the E-plane waveguide power divider/combiner in the proposed filter. The metal septum divides the input waveguide into two identical output waveguides. For high-order TE_{n0} modes, if the septum is thin enough, the power divider/combiner can achieve equal power splitting over a large bandwidth. On the other hand, by reducing the side size of the waveguide's output/input ports to more than half, the cutoff frequencies of other higher-order modes (such as TM_{0n}, TE_{0n} modes) can be significantly increased and therefore suppressed.

The main filter part actually consists of two identical corrugated waveguide filters (named as partial filters) that are mirror-symmetrical about the septum. As shown in Fig.1, the input/output port impedance of the partial filter is less than half of the input port impedance of the proposed filter. Therefore, additional impedance transformers are no longer required in the proposed waveguide filter, resulting in a compact size. It should also be emphasized that in the proposed filter, the two branch filters must be strictly symmetrical to

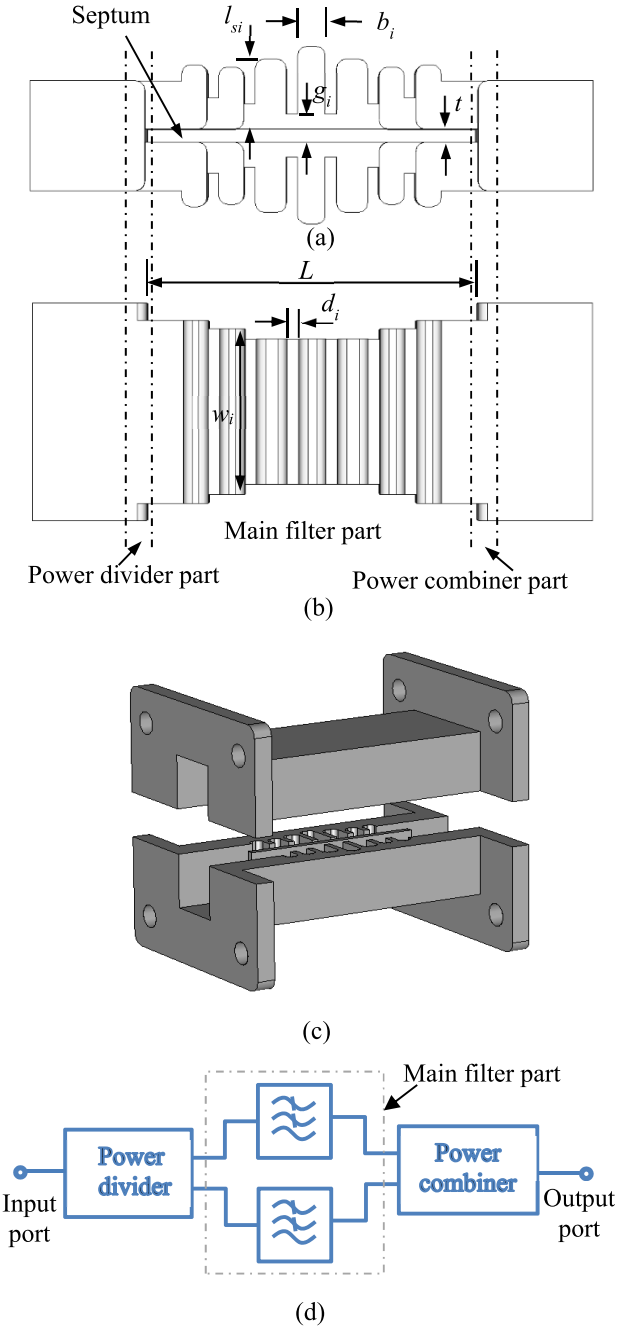

FIGURE 1. Structure of the proposed filter, (a) top view; (b) front view; (c) 3D view; (d) equivalent circuit model.

ensure that the signals are transmitted with the same phase shift in both branches.

B. MODE CONVERSION IN THE POWER DIVIDER/COMBINER PART

Many higher-order modes, such as TE_{01}, TE_{11} modes, cannot propagate in the output waveguides of the power divider due to their higher cutoff frequencies. However, if these modes are excited at the input port of the power divider, they can be converted to other modes and transmit into

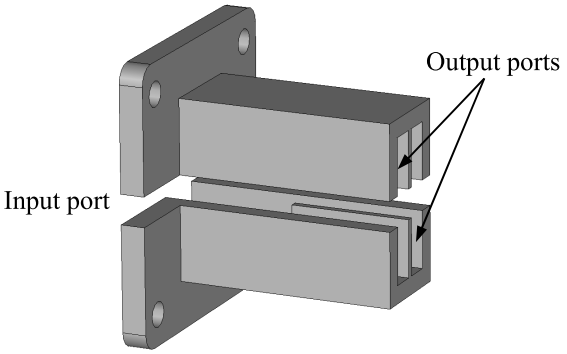

FIGURE 2. The structure of the power divider/combiner in the proposed filter.

the output waveguide. In this case, spurious components may be generated in the stopband. To analyze the characteristics of mode conversion in the power divider/combiner, a Ku-band power divider/combiner is designed as shown in Fig.2. The input port (port1) is with an dimension of 19.05 × 9.525 mm^2, while that of the output port (port2 and port3) is 19.05 × 4 mm^2. It can be calculated that only TE_{10}, TE_{20} and TE_{30} modes can propagate in the output waveguide below 30 GHz frequency, whereas there are 9 higher-order modes that can propagate in the input waveguide. The transmission characteristics of the designed power divider/combiner are analyzed by CST Microwave Studio. Simulation results indicate that, if the input port is excited by TE_{10} or TE_{20} or TE_{30} mode, good power division/combining performance can be obtained with nearly zero mode conversion. Meanwhile, simulation results also show that, almost all the energy of TE_{01} mode excited at the input port is reflected back, and only a tiny fraction is converted into the TE_{20} mode and then transmitted to the output ports. Fig.3 shows the simulation curves of the designed power divider/combiner excited by TE_{11}, TM_{11} and TE_{21}, TM_{21} at the input port, respectively. Obviously, high level mode conversion occurs. As shown in Fig.3(a), $|S_1(TE_{11}), {}_1(TE_{11})|$ decreases from 0 to −1.4 dB over the frequency range of 17.6-30 GHz, whereas $|S_1(TM_{11}), {}_1(TE_{11})|$ and $|S_2(TE_{10}), {}_1(TE_{11})|$ increase monotonically from −35 dB to −8.6 dB and −11.5 dB, respectively. It means that above the cutoff frequency of TE_{11} mode, more and more energy will be converted into TE_{10} and TM_{11} modes. They will transmit to the output ports, and then reflect back to the input port. Fig.3(a) also show that most of the energy of the TM_{11} mode is converted into TE_{10} mode and transmitted to the output port, whereas only a small part is converted into TE_{11} mode and reflected back to the input port. Although both TE_{11} mode and TM_{11} mode can be converted into TE_{10} mode, the field distribution in the waveguide of them is different. Therefore, their S-parameter curves are not the same. Similar mode conversions can be observed in Fig. 3(b), when the input port of the power divider/combiner is excited by the TE_{21} and TM_{21} modes.

Additionally, since many higher-order modes can be converted into TE_{n0} modes in the power divider, the spurious

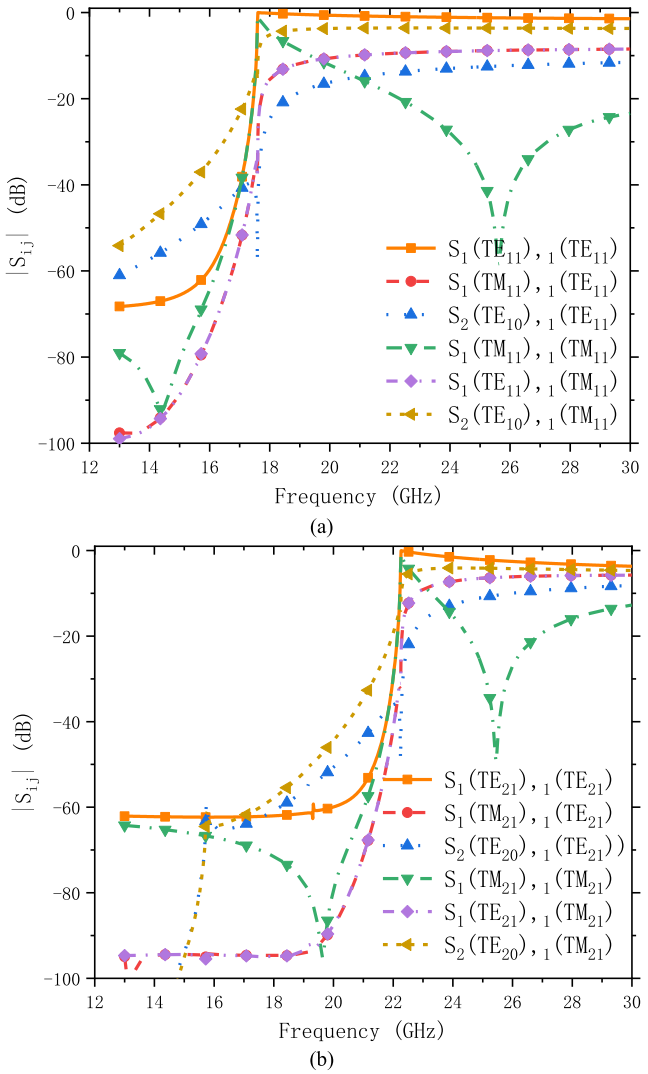

FIGURE 3. Mode conversion in the power divider part, (a) excited by TE11, TM11 modes, (b) excited by TE21, TM21 modes.

passband generated by the TE_{n0} mode in the stopband should be avoided as much as possible in the design of the main filter part.

C. FILTER DESIGN AND RESULTS

In order to suppress TE_{n0} modes over a wide stop-band, an inhomogeneous tapered corrugated structure is adopted to design the partial filter. As shown in Fig. 1(a), the narrow side dimension g_i of the partial filter is gradually decreased from the ends to the center, in order to eliminate the propagation of higher-order modes other than TE_{n0} modes. The detailed design method of the proposed filter is similar to that of the inhomogeneous tapered corrugated filter in [16] and will not be repeated here. Considering the discontinuity influence introduced by the thickness t of the septum on the reflection performance of TE_{10} mode as well as the difficulty in processing, the t value is set as 1.6 mm. Furthermore, as shown in Fig.1, to accommodate the actual machining process, all short-circuited waveguide stubs are chamfered by 0.8 mm.

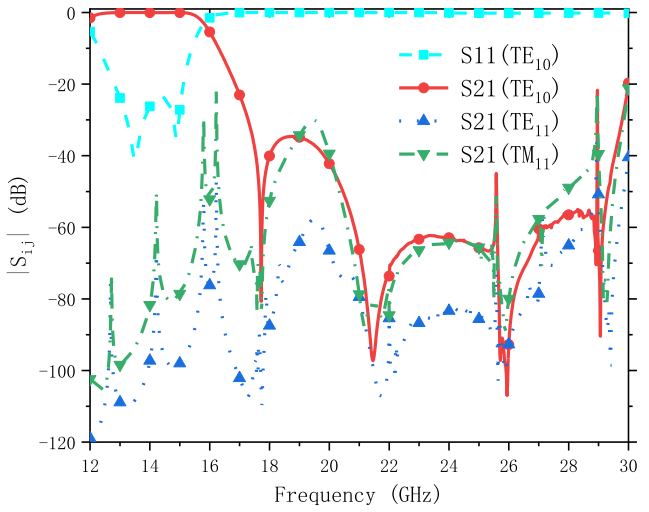

FIGURE 4. Simulation performance of designed filter for incident waves in the TE_{10} mode, TE_{11} mode, and TM_{11} mode.

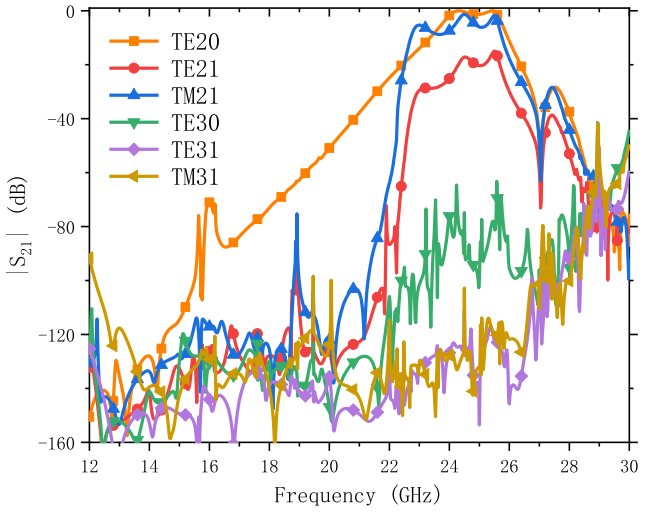

FIGURE 5. Simulation performance of designed filter for incident waves in the TE_{20} mode, TE_{21} mode, TM_{21} mode, TE_{30} mode, TE_{31} mode and the TM_{31} mode.

The filter is simulated and optimized using CST Microwave Studio. The simulation results validate that the proposed filter has good performance in TE_{10} mode. As shown in Fig.4, the reflection is less than −23dB among 13-15 GHz band, and the stop-band rejection is better than 35dB between 17.5-29.6 GHz, except for a narrow spike around 29 GHz. The filter responses in TE_{11} and TM_{11} modes are also given in Fig.4. Generally speaking, the stop band is free of spurious bands in the TE_{11} and TM_{11} modes, with only small narrow-band spikes due to mode conversion.

As mentioned in Section I, it is difficult to remove spurious bands or spikes in the stopband caused by the TE_{20} mode. Therefore, a spurious pass band with a center frequency of 25 GHz in the TE_{20} mode is observed in Fig.5. In the operating band of interest (27.5-29 GHz), the rejection of the TE_{20} mode is only better than 28 dB due to the spurious pass band. Moreover, as illustrated in the Section II-B,

the waves in the TE_{21} and TM_{21} modes cannot propagate through the partial filter, but they can be converted into the TE_{20} mode. Therefore, in Fig.5, the response curves of these spurious passbands are similar to each other shapes. The filter responses in the TE_{30}, TE_{31} and TM_{31} modes are also displayed in Fig.5. Apart from small spikes with amplitudes of −40 dB around 29 GHz, 'clean' out-of-band rejection is observed.

To obtain a wide rejection band, effective measures must be taken to suppress the spurious passband of the TE_{20} mode. A common approach is to increase the filter order. However, it comes at the cost of increasing the physical size. Furthermore, it should be mentioned that, the higher-order mode performances in Fig.5 are based on the worst case of incident waves with pure higher-order modes. In practical applications, the level of these higher-order modes may be considerably lower than that of the TE_{10} mode. If the amplitudes of the TE_{20}, TE_{21} and TM_{21} modes in the incident waves are small enough, a 'clean' rejection band can also be achieved.

III. REJECTION PERFORMANCE WITH THE E-PLANE M2W TRANSITION

M2W transitions are commonly used in power amplifiers, to transfer the quasi-TEM mode in microstrip line to TE_{10} mode in rectangular waveguide. However, in the harmonic frequency band, besides TE_{10} mode, higher-order modes are also excited in the waveguide. Compared with other transition structures, *E*-plane probe-type M2W transition [25], [26] has many unique advantages, such as low insertion loss, wide operating band, simple structure, and so on. Therefore, this M2W transition structure is employed in our power amplifier designed.

A. HIGHER-ORDER MODES GENERATED BY THE E-PLANE PROBE-TYPE M2W TRANSITION

To estimate the level of higher-order modes excited by the M2W transition, as shown in Fig.6, a Ku-band *E*-plane probe M2W transition is designed using WR-75 waveguide and Rogers RT6035HTC substrate ($\varepsilon_r = 3.6$) with a thickness of 0.254 mm. The performance of the M2W transition in the fundamental frequency band is also analyzed using CST Microwave Studio. There are totally 9 higher-order modes with cutoff frequencies below 30 GHz in the WR75 waveguide. Fig.7 shows the scattering parameters of these higher-order modes in the frequency range of 12.5∼30 GHz. In this case, $|S_{21}|$ of $TE_{\rm nm}$ means the response at port 2 in $TE_{\rm nm}$ mode due to a quasi-TEM mode signal at port 1. It can be seen that only TE_{10} mode is excited below the frequency of 15 GHz, whereas TE_{11}, TM_{11}, TE_{30}, TE_{31} and TM_{31} modes are excited above their cutoff frequencies.

As shown in Fig.7, the maximum $|S_{21}|$ of these five higher-order modes is about −5 dB. Theoretically, if the *E*-plane M2W transition is with symmetry structure, TE_{20}, TE_{21} and TM_{21} modes cannot be excited. However, the asymmetry is introduced by the window in the broadside wall and the introduced by the window in the broadside wall and the substrate inserted into the waveguide. Therefore, these higher-order modes are also excited, but are with relatively small levels. As shown in Fig.7, the maximum $|S_{21}|$ of the TE_{20}, TE_{21} and TM_{21} modes is −25 dB, −22 dB and −38 dB, respectively.

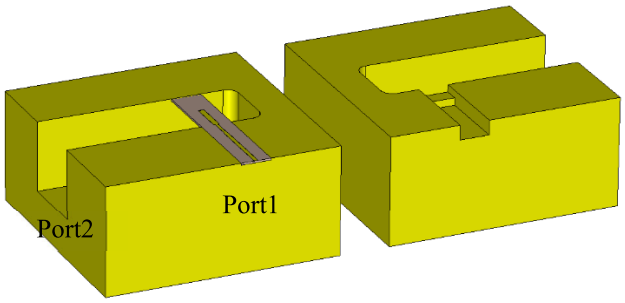

FIGURE 6. Ku-band M2W transition.

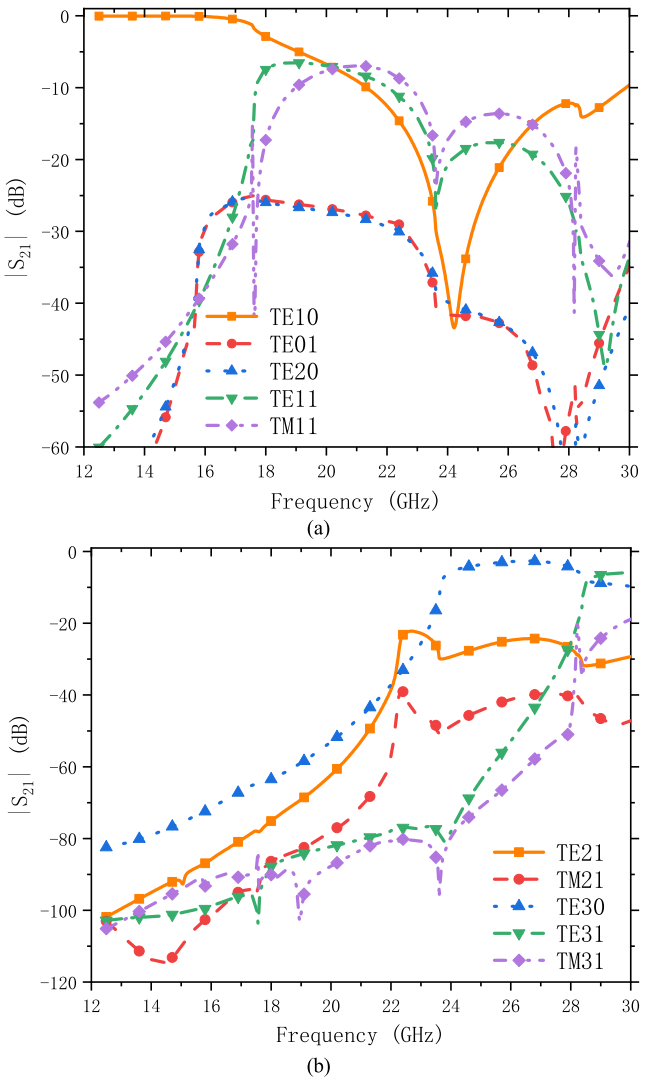

FIGURE 7. Simulation results of the designed M2W transition, (a) $|S_{21}|$ of TE_{10}, TE_{20}, TE_{01}, TE_{11} and TM_{11} modes; (b) $|S_{21}|$ of TE_{21}, TM_{21}, TE_{30}, TE_{31} and TM_{31} modes.

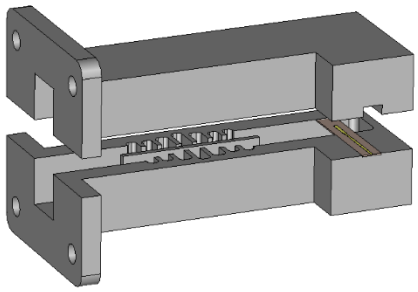

FIGURE 8. The proposed filter with the M2W.

B. PERFORMANCE OF THE FILTER WITH THE M2W TRANSITION

As the incident waves of the filter designed in this paper come from the output port of the M2W transition, it can be seen from Fig.7 that the amplitudes of the TE_{20}, TE_{21} and TM_{21} modes in the incident waves are relatively small. The proposed filter with the M2W transition in Fig.8 is analyzed by CST Microwave Studio. As shown in Fig.9, the M2W transition has a little effect on the filter performance in the pass band. Additionally, the stop band performance of the higher-order modes is greatly improved. Instead of spurious passbands, several spikes with amplitudes of about −20 dB are observed around 25GHz. Spikes around 22 GHz and 27 GHz are also observed, because of the higher-order mode impedance mismatch between the filter and M2W transition. The rejection of the higher-order modes is better than 50 dB in the frequency band of 27.5-29 GHz. Apparently, this improvement is attributed to the higher-order modes suppression of the M2W transition. The spike amplitudes of the TE_{20}, TE_{21} and TM_{21} modes depend on the rejection values of these modes. Therefore, a greater improvement can be obtained by using a M2W transition structure with better symmetry such as the structure proposed in reference [26].

C. MEASURED RESULTS OF THE DESIGNED FILTER

As shown in Fig.10, the designed filter was milled symmetrically along the center line of the broadside wall using a common computer-controlled milling process, and fastened with mounting screws. To reduce the insertion loss, the surface of the fabricated filter is silver-plated. The effective length of the filter L is 29 mm and the total length is 50 mm. The minimum gap of the filter is 1.3 mm, which means that the peak power-handling capacity of the designed filter at normal atmospheric pressure and room temperature is about 20 kW [13].

The filter is measured using a Keysight E8364C vector network analyzer and coaxial-to-waveguide (WR-75) adapters. To obtain the filter response excited by a signal similar to the M2W transition output, the waveguide taper is not used in the measurements. Due to the lack of a waveguide calibration kit, the reference plane for the measurement is at the SMA port of the coaxial-to-waveguide adapter. Fig.11 shows the

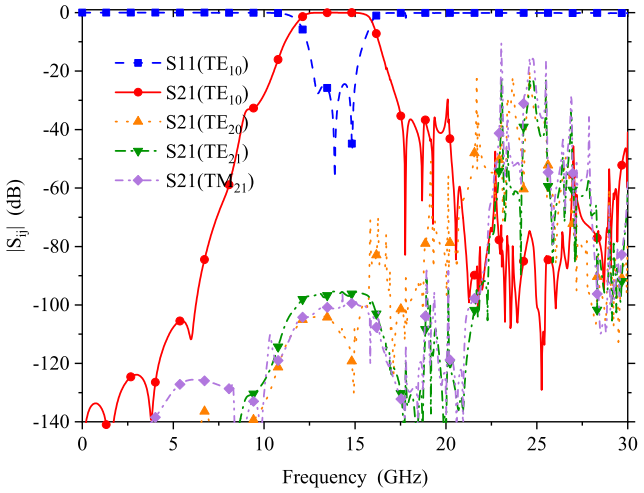

FIGURE 9. Simulation results of the proposed filter with the M2W.

FIGURE 10. Picture of the fabricated filter.

measured results. It indicates that the reflection coefficient is better than −17 dB and the insertion loss is less than 0.8 dB over the frequency range from 13.75 to 14.5 GHz. It should be noted that the measured insertion loss of the filter includes a loss of about0.7 dB that introduced by the back-to-back coaxial-to-waveguide adapter. Therefore, the loss of the filter is less than 0.1 dB. It is observed from Fig.11 that, there are no spurious pass-bands below 30 GHz, but only several narrow band spikes. Additionally, the rejection is better than 50 dB in the 27-29.5 GHz, except for two spikes around 27.8 GHz and 29 GHz, respectively. From the measured results, it can be calculated that the shape factor, which is defined as the ratio of the 30 dB rejection bandwidth to the 3 dB bandwidth, of the proposed filter is approximately 1.94. Compared with some waveguide filters [27], [28], the shape factor of the proposed filter is not very good. However, these waveguide filters [27], [28] suffer from narrow stopband performance and cannot be used for harmonic rejection applications. The test results are in good agreement with the previous analysis and simulated results. It should be noted that in simulation, the excitation is in quasi-TEM mode, while the output signal is in waveguide mode. In the measurements, both the input and output signals are in TEM mode. This may be the main reason for the small deviation between simulated and measured results.

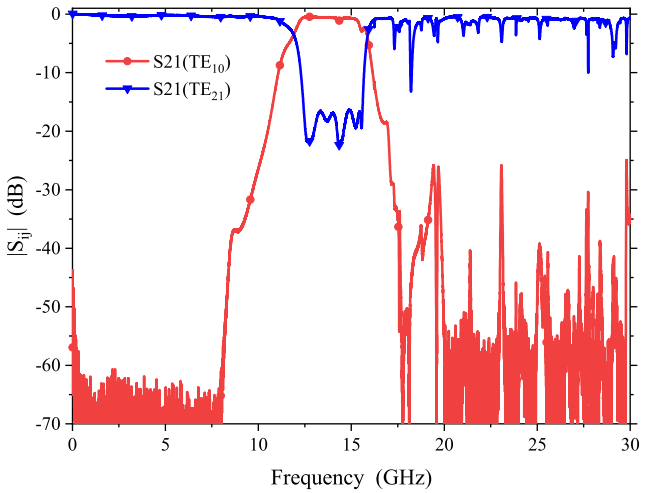

FIGURE 11. Measured performance of the designed filter.

Comparisons of the proposed filter with other published waveguide filters are summarized in Table 1. The results demonstrate that the filter developed in this work achieves the most compact size and the lowest insertion loss performance compared to its counterparts.

IV. HARMONIC REJECTION OF THE POWER AMPLIFIER WITH THE DESIGNED FILTER

The above analysis shows that the proposed filter is very suitable for the harmonic rejection of power amplifiers. As a practical and straightforward demonstration, a Ku-band power amplifier module in the same operating band of 13.75∼14.5 GHz is designed using GaN MMICs. The input/output port of the power amplifier is WR-75 waveguide, and the M2W transition designed in Section II-A is used as interconnection between the microstrip line and rectangular waveguide. The output power and second harmonic rejection performances of the designed power amplifier module are measured. The test schematic is shown in Fig.12. A Keysight E8267D signal generator is used to provide excited signal. Due to the limited output power of the E8267D, a driver amplifier with P_{out1dB} of 30 dBm is used in the test. A 30 dB waveguide coupler is used, which transmits the output power to the spectrum analyzer (Rohde & Schwarz FSW50) or power meter (Keysight N1912+N1922). The through port of the coupler is terminated with a high-power load. The spectrum analyzer is used to measure the second harmonic rejection performance of the amplifiers in saturation state, and the power meter is used to measure the saturated output power. As shown in Fig.13, the saturated output power in the 13.75∼14.5 GHz frequency band exceeds 48.6 dBm (72.5W) and the minimum 2nd harmonic rejection is about 20 dBc. To improve the 2nd harmonic rejection performance of the power amplifier, the proposed filter is added between the power amplifier and the 30 dB waveguide coupler in the measurement. For a clear comparison, the measured results in this case are also added in the Fig.13. The saturated output power is reduced only by about 0.1 dB due to the insertion loss of the proposed filter. However, by employing the harmonic reject filter, the 2nd harmonic rejection is better than 60 dBc in the frequency band of 13.75∼14.0 GHz and 14.1∼14.5 GHz, respectively. Meanwhile, the rejection is about 52 dBc between 14.0∼14.1 GHz, which may be caused by the spike in the filter response around 28 GHz. These results agree well with the measured results of the filter in Fig.11.

TABLE 1. Filter comparision.

Ref.	Passband	Insertion Loss(dB)	Ratio*	Length
Filter in [17]	10.7-12.7	≤ 0.1	3.41	$5.85\lambda_0$
Filter in [22]	10.7-12.7	≤0.5	3.41	10.73
Filter in [23]	17.5-21.5	≤0.25	3.58	$8.46\lambda_0$
This Work	12.7-15	≤0.1	2.17	$1.34\lambda_0$

*Ratio is defined as the ratio of upper stopband frequency to the center frequency.

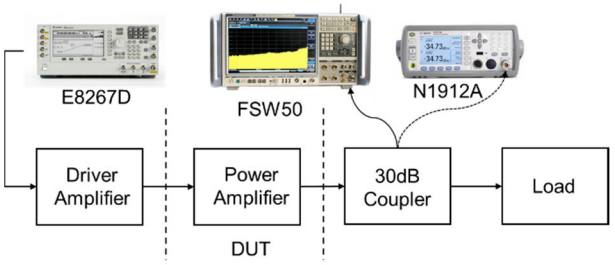

FIGURE 12. Test schematic of the Ku-band power amplifier.

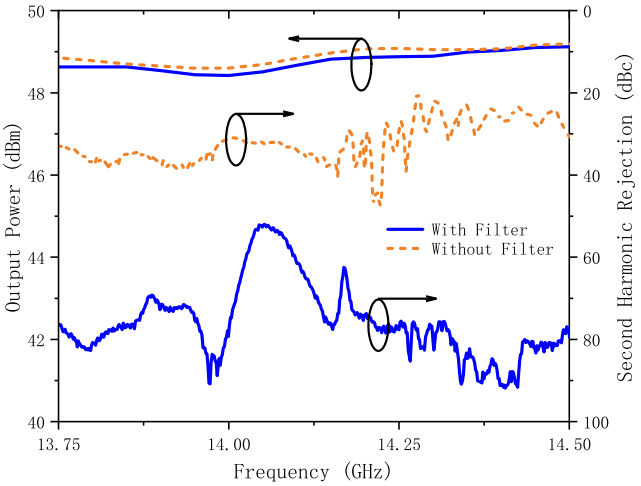

FIGURE 13. Performance of the Ku-band amplifier with and without filter.

V. CONCLUSION AND DISCUSSION

In this paper, a novel miniaturized low-pass waveguide filter for harmonic rejection application is proposed. To validate the proposed concept, a Ku-band harmonic reject filter is designed. The effective length of the filter is only 29 mm. To give a practical and straightforward demonstration, a Ku-band RF transmitter prototype, which composed of a power amplifier module and the proposed filter, is designed and

measured. Measured results show that the transmitter has a minimum output power of 70 W and a 2nd harmonic rejection better than 52 dBc. Compared with the case without the filter, the output power is reduced only by 0.1 dB, while the 2nd harmonic rejection performance is improved by 30 dB.

Simulation results show that a wide stop-band of the proposed filter is obtained in TE_{10} mode. Although inhomogeneous tapered corrugated filter structure is adopted in this filter design, spurious pass-bands in TE_{20}, TE_{21} and TM_{21} are observed in the stop-band. The mode conversion analysis shows that, the spurious pass-bands in TE_{21} and TM_{21} modes are caused by that of the TE_{20} mode. Therefore, if the partial filter is designed using composite corrugated filter structure [17], the proposed filter will achieve a broadband stop-band without spurious pass-bands in all modes.

On the other hand, simulation results show that the spurious pass-bands performance of the proposed filter can be improved by using E-plane probe-type M2W transition. However, this improvement is limited because the minimum suppression of the designed M2W transition in TE_{20}, TE_{21} and TM_{21} modes is about 22 dB. A greater improvement can be obtained by using a M2W transition structure with better symmetry.

REFERENCES

[1] Y. Ma, H. Jiang, J. Li, H. Yu, C. Li, and D. Zhang, "Design of marine satellite communication system based on VSAT technique," in *Proc. Int. Conf. Comput., Internet Things Control Eng. (CITCE)*, Nov. 2021, pp. 126–129.

[2] C. B. Nelson, B. D. Steckler, and J. A. Stamberger, "The evolution of hastily formed networks for disaster response: Technologies, case studies, and future trends," in *Proc. IEEE Global Humanitarian Technol. Conf.*, Oct. 2011, pp. 467–475.

[3] A. Garcia-Dominguez, "Mobile applications, cloud and bigdata on ships and shore stations for increased safety on marine traffic; a smart ship project," in *Proc. IEEE Int. Conf. Ind. Technol. (ICIT)*, Mar. 2015, pp. 1532–1537.

[4] P. Kim, I.-K. Lee, D.-G. Oh, and J.-G. Ryu, "Robust initial access technique of spread spectrum based on DVB-RCS2 standard for mobile application," in *Proc. 36th Int. Satell. Commun. Syst. Conf. (ICSSC)*, 2018, pp. 1–5.

[5] T. Yoshioka, K. Harauchi, T. Sugitani, T. Yamasaki, H. Ichinohe, M. Miyashita, K. Yamamoto, and S. Goto, "A Ku-band 70-W class GaN internally matched high power amplifier with wide offset frequencies of up to 400 MHz for multi-carrier satellite communications," in *Proc. IEEE BiCMOS Compound Semiconductor Integr. Circuits Technol. Symp. (BCICTS)*, Nov. 2020, pp. 1–4.

[6] G. Maral, *VAST Networks*, 2nd ed. Hoboken, NJ, USA: Wiley, 2003.

[7] H. Wei, L. Shen, and D. Wang, "Current situation and development trend of 5G millimeter wave," in *Proc. Manage. Sci. Informatization Econ. Innov. Develop. Conf. (MSIEID)*, Dec. 2020, pp. 322–325.

[8] W. H. Bailey, B. R. T. Cotts, and P. J. Dopart, "Wireless 5G radiofrequency technology—An overview of small cell exposures, standards and science," *IEEE Access*, vol. 8, pp. 140792–140797, 2020.

[9] V. E. Boria and B. Gimeno, "Waveguide filters for satellites," *IEEE Microw. Mag.*, vol. 8, no. 5, pp. 60–70, Oct. 2007.

[10] Z. Xu, J. Guo, C. Qian, and W.-B. Dou, "A novel quasi-elliptic waveguide transmit reject filter for Ku-band VSAT transceivers," *Prog. Electromagn. Res.*, vol. 117, pp. 393–407, 2011.

[11] F. M. Vanin, D. Schmitt, and R. Levy, "Dimensional synthesis for wide-band waveguide filters and diplexers," *IEEE Trans. Microw. Theory Techn.*, vol. 52, no. 11, pp. 2488–2495, Nov. 2004.

[12] E. D. Sharp, "A high-power wide-band waffle-iron filter," *IEEE Trans. Microw. Theory Techn.*, vol. MTT-11, no. 2, pp. 111–116, Mar. 1963.

[13] R. Levy, "Tapered corrugated waveguide low-pass filters," *IEEE Trans. Microw. Theory Techn.*, vol. MTT-21, no. 8, pp. 526–532, Aug. 1973.

[14] M. Yang, H. Wang, T. Yang, B. Hu, H. Li, Y. Zhou, and T. Li, "Design of wide stopband for waveguide low-pass filter based on circuit and field combined analysis," *IEEE Microw. Wireless Compon. Lett.*, vol. 31, no. 11, pp. 1199–1202, Nov. 2021.

[15] W. Hauth, R. Keller, and U. Rosenberg, "CAD of waveguide low-pass filters for satellite applications," in *Proc. 17th Eur. Microw. Conf.*, Rome, Italy, Oct. 1987, pp. 151–156.

[16] R. Levy, "Inhomogeneous stepped-impedance corrugated waveguide low-pass filters," in *IEEE MTT-S Int. Microw. Symp. Dig.*, vol. 2005, pp. 123–126.

[17] F. De Paolis, R. Goulouev, J. Zheng, and M. Yu, "CAD procedure for high-performance composite corrugated filters," *IEEE Trans. Microw. Theory Techn.*, vol. 61, no. 9, pp. 3216–3224, Sep. 2013.

[18] A. M. K. Saad, "Novel lowpass harmonic filters for satellite application," in *IEEE MTT-S Int. Microw. Symp. Dig.*, May 1984, pp. 292–294.

[19] A. Kirilenko, L. Rud', V. Tkachenko, and D. Kulik, "Design of bandpass and lowpass evanescent-mode filters on ridged waveguides," in *Proc. 29th Eur. Microw. Conf.*, Oct. 1999, pp. 239–242.

[20] I. Arregui, I. Arnedo, A. Lujambio, M. Chudzik, D. Benito, R. Jost, F. J. Gortz, T. Lopetegi, and M. A. G. Laso, "A compact design of high-power spurious-free low-pass waveguide filter," *IEEE Microw. Wireless Compon. Lett.*, vol. 20, no. 11, pp. 595–597, Nov. 2010.

[21] I. Arregui, F. Teberio, I. Arnedo, A. Lujambio, M. Chudzik, D. Benito, R. Jost, F. J. Gortz, T. Lopetegi, and M. A. G. Laso, "High-power low-pass harmonic waveguide filter with TE_{n0}-mode suppression," *IEEE Microw. Wireless Compon. Lett.*, vol. 22, no. 7, pp. 339–341, Jul. 2012.

[22] I. Arregui, F. Teberio, I. Arnedo, A. Lujambio, M. Chudzik, D. Benito, T. Lopetegi, R. Jost, F.-J. Gortz, J. Gil, C. Vicente, B. Gimeno, V. E. Boria, D. Raboso, and M. A. G. Laso, "High-power low-pass harmonic filters with higher-order TE_{n0} and non-TE_{n0} mode suppression: Design method and multipactor characterization," *IEEE Trans. Microw. Theory Techn.*, vol. 61, no. 12, pp. 4376–4386, Dec. 2013.

[23] F. Teberio, I. Arregui, A. Gomez-Torrent, E. Menargues, I. Arnedo, M. Chudzik, M. Zedler, F. J. Görtz, R. Jost, T. Lopetegi, and M. A. G. Laso, "High-power waveguide low-pass filter with all-higher-order mode suppression over a wide-band for Ka-band satellite applications," *IEEE Microw. Wireless Compon. Lett.*, vol. 25, no. 8, pp. 511–513, Aug. 2015.

[24] F. Teberio, I. Arregui, A. Gomez-Torrent, E. Menargues, I. Arnedo, M. Chudzik, M. Zedler, F. J. Görtz, R. Jost, T. Lopetegi, and M. A. G. Laso, "Chirping techniques to maximize the power-handling capability of harmonic waveguide low-pass filters," *IEEE Trans. Microw. Theory Techn.*, vol. 64, no. 9, pp. 2814–2823, Sep. 2016.

[25] Y. C. Leong and S. Weinreb, "Full band waveguide-to-microstrip probe transitions," in *IEEE MTT-S Int. Microw. Symp. Dig.*, Anaheim, CA, USA, Jun. 1999, pp. 1435–1438.

[26] Y.-C. Shih, T.-N. Ton, and L. Q. Bui, "Waveguide-to-microstrip transitions for millimeter-wave applications," in *IEEE MTT-S Int. Microw. Symp. Dig.*, May 1988, pp. 473–475.

[27] L. Pelliccia, C. Tomassoni, F. Cacciamani, P. Vallerotonda, R. Sorrentino, J. Galdeano, and C. Ernst, "Very-compact waveguide bandpass filter based on dual-mode TM cavities for satellite applications in Ku-band," in *Proc. 48th Eur. Microw. Conf. (EuMC)*, Sep. 2018, pp. 93–96.

[28] A. R. Eskandari, A. Kheirdoost, and M. Haghparast, "Improvement of passband flatness for a compact, narrowband, and highly selective TM dual-mode filter," *IEEE Trans. Microw. Theory Techn.*, vol. 68, no. 4, pp. 1591–1597, Apr. 2020.

XUEJIAN JIANG was born in Shaanxi, China. He received the B.S. degree from Xidian University, Xi'an, China, in 2020. He is currently pursuing the M.S. degree in electromagnetic field and microwave technology with Southeast University, Nanjing, China.

His current research interest includes microwave and millimeter-wave components.

ZHENGBIN XU was born in Anhui, China. He received the B.S. degree from Xidian University, Xi'an, China, in 2004, and the M.S. and Ph.D. degrees in electrical engineering from Southeast University (SEU), Nanjing, China, in 2007 and 2012, respectively.

Since 2012, he has been with the State Key Laboratory of Millimeter Waves, SEU, where he is currently a Research Assistant. He has authored or coauthored over 20 refereed journals and conference papers. His current research interests include microwave and millimeter-wave components, and subsystems for radar and communication applications.

JIE XU received the B.S., M.S., and Ph.D. degrees in electrical engineering from Southeast University (SEU), Nanjing, China, in 2008, 2011, and 2017, respectively.

In 2018, he joined the School of Information Science and Engineering, SEU, as a Postdoctoral Researcher. His research interests include microwave and millimeter-wave circuits, metamaterial structures, and antennas design.

JIAN GUO (Member, IEEE) was born in Yangzhou, Jiangsu, China, in 1982. He received the B.S. degree in information engineering and the Ph.D. degree in electromagnetic and microwave technology from Southeast University (SEU), Nanjing, China, in 2005 and 2012, respectively.

He is currently with the State Key Laboratory of Millimeter Waves, SEU. His main research interests include millimeter-wave and terahertz circuits.

CHENG QIAN received the B.E. and M.E. degrees in radio engineering from Southeast University (SEU), Nanjing, China.

He is currently involved in research and teaching of microwave and millimeter-wave technology with the State Key Laboratory of Millimeter Wave, SEU.